THE JOURNAL OF PHYSICAL CHEMISTRY A
A JOURNAL OF THE AMERICAN CHEMICAL SOCIETY

pubs.acs.org/JPCA

Article

Molecular Cage Reports on Its Contents: Spectroscopic Signatures of Cryo-Cooled K^+- and Ba^{2+}-Benzocryptand Complexes

Published as part of The Journal of Physical Chemistry virtual special issue "Marsha I. Lester Festschrift".

Casey D. Foley, Cole D. Allen, Kendrew Au, Chin Lee, Susan B. Rempe, Pengyu Ren, Edwin L. Sibert, III,* and Timothy S. Zwier*

Cite This: *J. Phys. Chem. A* 2023, 127, 6227−6240

Read Online

ACCESS | Metrics & More | Article Recommendations | Supporting Information

ABSTRACT: UV photofragment spectroscopy and IR−UV double resonance methods are used to determine the structure and spectroscopic responses of a three-dimensional [2.2.2]-benzocryptand cage to the incorporation of a single K^+ or Ba^{2+} imbedded inside it (labeled as K^+-BzCrypt, Ba^{2+}-BzCrypt). We studied the isolated ion-cryptand complex under cryo-cooled conditions, brought into the gas phase by nano-electrospray ionization. Incorporation of a phenyl ring in place of the central ethyl group in one of the three N-CH_2-CH_2-O-CH_2-CH_2-O-CH_2-CH_2-N chains provides a UV chromophore whose S_0−S_1 transition we probe. K^+-BzCrypt and Ba^{2+}-BzCrypt have their S_0−S_1 origin transitions at 35,925 and 36,446 cm^{-1}, respectively, blue-shifted by 174 and 695 cm^{-1} from that of 1,2-dimethoxybenzene. These origins are used to excite a single conformation of each complex selectively and record their IR spectra using IR−UV dip spectroscopy. The alkyl CH stretch region (2800−3000 cm^{-1}) is surprisingly sensitive to the presence and nature of the encapsulated ion. We carried out an exhaustive conformational search of cage conformations for K^+-BzCrypt and Ba^{2+}-BzCrypt, identifying two conformations (A and B) that lie below all others in energy. We extend our local mode anharmonic model of the CH stretch region to these strongly bound ion-cage complexes to predict conformation-specific alkyl CH stretch spectra, obtaining quantitative agreement with experiment for conformer A, the gas-phase global minimum. The large electrostatic effect of the charge on the O- and N-lone pairs affects the local mode frequencies of the CH_2 groups adjacent to these atoms. The localized CH_2 scissors modes are pushed up in frequency by the adjacent O/N-atoms so that their overtones have little effect on the alkyl CH stretch region. However, the localized CH_2 wags are nearly degenerate and strongly coupled to one another, producing an array of delocalized wag normal modes, whose highest frequency members reach up above 1400 cm^{-1}. As such, their overtones mix significantly with the CH stretch modes, most notably involving the CH_2 symmetric stretch fundamentals of the central ethyl groups in the all-alkyl chains and the CH stretches adjacent to the N-atoms and antiperiplanar to the nitrogen lone pair.

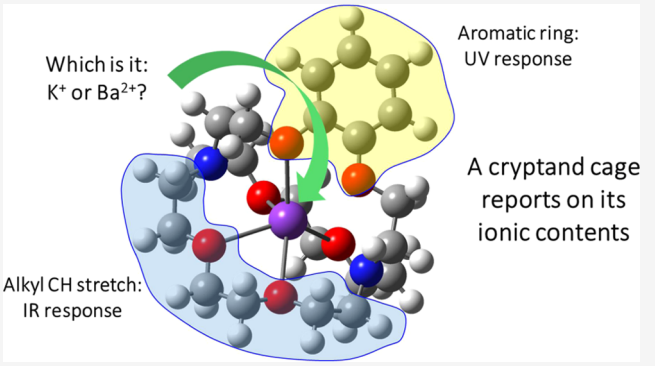

I. INTRODUCTION

The field of supramolecular chemistry has its genesis in molecular cages such as cryptands that are designed to selectively trap ions by size, charge state, and binding geometry.[1,2] The [2.2.2]cryptand cage is prototypical (Figure 1a), with its three di-ether bridges connected to one another by two capping tertiary amines. These cages are highly soluble in water. A single alkali metal or alkaline earth cation fits snugly inside the cryptand cage (Figure 1b), bound by the lone pairs from six oxygens with secondary interactions with the two capping nitrogen lone pairs. Binding energies for ions of appropriate size to the cage are sufficiently strong that they compete with aqueous solvation of the ions, enabling effective capture of ions from aqueous solution.

Since their inception, cryptands have been widely used for selective ion capture, and a variety of synthetic strategies have been employed to incorporate various functional groups/spacers in the cage, changing its cavity size and enabling trapping of an impressive number of atomic cations and anions, ion pairs, and a variety of ion-H_2O complexes.[1,3] The three-dimensional (3D) cage structures of the cryptands constitute an extraordinary platform for studying the

Received: May 22, 2023
Revised: July 6, 2023
Published: July 21, 2023

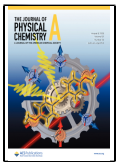

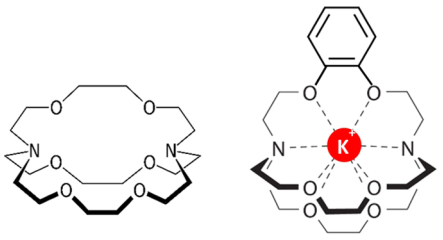

(a) [2.2.2]cryptand (b) K^+-[2.2.2]benzocryptand

Figure 1. Chemical structures of (a) [2.2.2]cryptand and (b) K^+-[2.2.2]benzocryptand.

spectroscopic effects of nanoconfinement.[4] Typically, studies of nanoconfinement concentrate on the confined species, treating the confining media as immutable. However, cryptands are molecular-scale 3D cages that can flex and respond to their contents, and the bridging chains can possess spectroscopic probes that report on confinement from the perspective of the cage.

Much of the knowledge about these cryptand complexes in prior work comes from X-ray spectra of the ion-imbedded cages in crystalline form. Thus, the X-ray structures are known for the series of alkali metal and alkaline earth cations in [2.2.2]cryptand with various counterions.[5−12] Since cryptands capture ions, they are also ready targets of mass spectrometry.[13,14] This enables the study of the ion-cage complexes free from solvent or packing effects, where mass spectrometry methods can provide binding energies and collisional fragmentation patterns. However, structural specificity is lacking, pointing to the need for spectroscopy of the gas-phase ion-cage complexes. Indeed, previous studies have probed the spectroscopy of crown ethers[15−24] and spherands[25] bound to alkali and alkaline earth cations.

To obtain a deeper understanding of the binding of ions to the [2.2.2]cryptand cage, we substitute a phenyl ring in place of one of the central ethyl groups, forming [2.2.2]-benzocryptand[26,27] (Figure 1b). This substitution provides an ultraviolet chromophore that will report on its ionic contents through its electronic spectrum. By cooling the gas-phase ion-cage complexes in a cryo-cooled ion trap, the population is brought to the zero-point levels of low-lying conformational minima, both simplifying and sharpening spectra.[28−31] Infrared spectra of the ions will produce complementary information regarding the structure and mode of binding. However, when applied to ions of sufficient size, the infrared spectrum can have contributions from more than one conformational isomer. The spectra due to individual conformations can be sorted out via IR−UV double resonance spectroscopy.[15,30,32]

In this work, we report infrared and ultraviolet spectra of cryo-cooled, gas-phase K^+-BzCrypt and Ba^{2+}-BzCrypt complexes. These ions form an interesting pair, as they are nearly identical in size[33] but differ in charge by a factor of two. Both ions fit optimally and selectively into the [2.2.2]cryptand cage, so much so that its trade name is Kryptofix 222.[34] Incorporating a phenyl ring into one of the ether bridges imbues one of the walls of the cryptand cage with an aromatic chromophore that provides a strong UV absorption similar to that of 1,2-dimethoxybenzene (DMB).[35,36] Two of the six ether oxygens are directly bonded to the phenyl ring, bringing some asymmetry to the binding pocket but also providing a UV spectroscopic signature of the way in which the cryptand cage responds to and reports on its contents. As we shall see, the UV photofragment spectra show both a significant shift to the blue in going from K^+ to Ba^{2+} but also display unique low-frequency Franck−Condon activity that reflects the response of the ion and cage to electronic excitation of the phenyl ring.

We also use IR−UV double resonance to record single-conformation IR spectra in the alkyl CH stretch region. In the context of other conformationally complex ions, IR spectra in the NH and OH stretch regions report directly on the H-bonding architecture of the ions.[29−31] However, compared to these structurally informative hydride stretch vibrations, the alkyl CH stretch transitions offer a much less well resolved or easily interpretable set of IR absorbers. There are several reasons for this. First, the CH_2 groups are, at best indirect probes of the binding to the ion, since the alkyl chains do not themselves directly engage in H-bonds or other strong interactions. Second, the alkyl CH stretch transitions appear in a rather narrow band in the IR (2800−3000 cm^{-1}), causing significant overlap in IR transitions. Third, this overlap is especially prevalent because the [2.2.2]benzocryptand cage is replete with alkyl CH_2 groups (a total of 16 of them), leading to 32 IR active CH stretch modes. Finally, the alkyl CH stretch modes experience pervasive and strong Fermi resonances with the overtones of the CH bends (called "scissors" modes in CH_2 groups), leading to splitting and intensity borrowing that render a harmonic analysis completely inadequate.[37] In such circumstances, it would seem ill-advised to use the CH stretch region as a structural diagnostic.

Nevertheless, this region is information-rich if it can be interpreted. Indeed, over the past several years, we have developed and refined an anharmonic local mode model of the alkyl CH stretch region,[37] successfully applying it to single-conformation IR spectra of pure alkyl chains,[37−41] cyclic alkanes,[42] methyl groups,[43] hydrocarbon radicals,[44,45] and alkyl ethers.[46] What is lacking to date is the extension of this model to strong-binding circumstances such as is present in the K^+/Ba^{2+}-benzocryptands. The present work demonstrates that the alkyl CH stretch transitions of the M^{+n}-BzCrypt complexes show surprising sensitivity to the charge state and mode of binding of the ion imbedded inside the cryptand cage. To account for these spectra and obtain firm assignments for the cage conformation, significant further development of the model was required, involving inclusion of the CH_2 wags and twists, which in other circumstances are too low in frequency to affect the CH stretch region.

II. EXPERIMENTAL METHODS

The experimental work was carried out in an apparatus that has been described previously.[29] Aspects unique to this study are emphasized here. Nano-electrospray ionization was used to bring the M^{+n}-BzCrypt complexes into the gas phase. The BzCrypt sample was available commercially. It was dissolved in a 50:50 H_2O/CH_3OH solution at 100 μM concentration. The KCl or barium acetate salts were dissolved separately and added to the mixture in some excess, ranging from 1:1 to 8:1 ratio of M^{+n}:BzCrypt. This produced a clean source of the K^+-BzCrypt (m/z 463) or Ba^{2+}-BzCrypt (m/z 286) complexes. In the latter complexes, if this solution sat for several days, it tended to produce higher concentrations of the Ba^{2+}-BaCrypt-Ac^{-1} complexes at m/z 621. As a result, we tended to use freshly prepared samples with concentrations of $Ba(Ac)_2$ closer to 1:1.

Ions from the electrospray source were stored in a linear quadrupole ion trap (QIT) before mass selection of the parent

https://doi.org/10.1021/acs.jpca.3c03457
J. Phys. Chem. A 2023, 127, 6227−6240

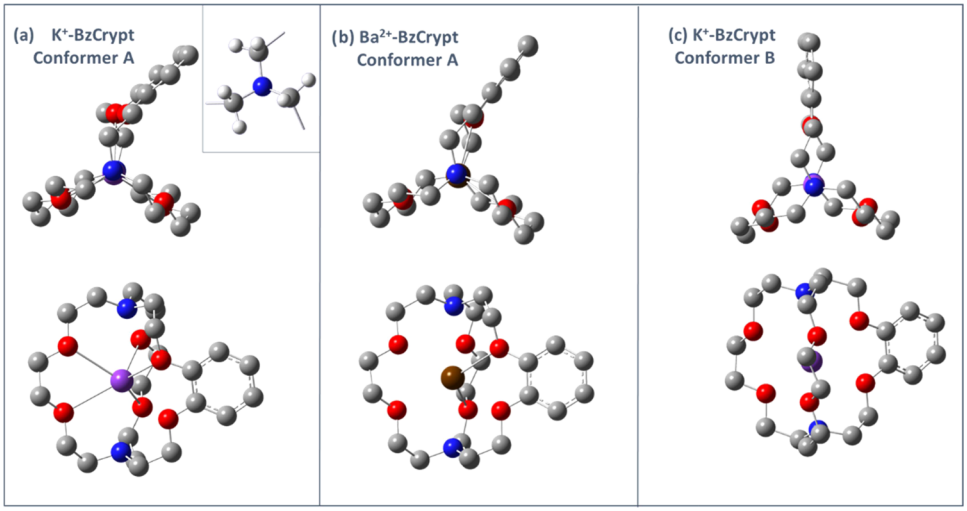

Figure 2. End-on (top) and side views of optimized structures for the global minima (conformer A) of (a) K^+-BzCrypt and (b) Ba^{2+}-BzCrypt complexes and (c) the second lowest energy structure of K^+-BzCrypt (conformer B), with hydrogens hidden for clarity. The inset in panel (a) shows a cutout of the CH_2 groups adjacent to the nitrogens with hydrogens included. The CH groups pointing out of the page (axial) are calculated to be the lowest frequency CH stretch modes in the cryptand cage. See text for further discussion.

ion of interest using rf/dc (apex) isolation.[47] This process also serves as an annealing step, as the parent ion is placed near the stability limit, where it experiences annealing collisions with the trapping gas (helium). The mass-selected ions are transported to an octupole ion trap cooled by a closed cycle refrigerator to 5 K. Helium pulsed into the trap serves as trapping gas and a mechanism for cooling the internal degrees of freedom of the ions.

UV photofragment spectra were recorded using the doubled output of a Nd:YAG pumped dye laser (Coumarin 540A) covering the 35,400−37,500 cm^{-1} region. UV excitation leads to photofragmentation of a few percent of the parent ions in the octupole trap. The ion mixture is released from the trap to an analysis linear QIT that operates in one of two modes. When recording a UV spectrum, resonant ejection is used to selectively remove parent ions from the trap ("parent knock-out") prior to collection of all remaining UV photofragment ions independent of their mass. Alternatively, the mass spectrum of the photofragment ions can be recorded at a fixed UV wavelength.

IR−UV double resonance is used to record ground-state infrared spectra via one of two methods. Infrared ion dip spectra are recorded by fixing the UV wavelength on a single vibronic transition of the parent ion so that the photofragment ion signal is due to the single conformation responsible for this absorption. A tuned IR source (LaserVision OPO/OPA) is spatially overlapped with the UV laser in the cold ion trap, but temporally preceding the UV by ∼100 ns. In the present work, overview IR spectra in the 2400−3800 cm^{-1} region were supplemented with shorter scans in the alkyl CH stretch region (2800−3000 cm^{-1}). When the IR wavelength is resonant with a vibrational transition of the monitored conformation of the ion, absorption will remove the population from the vibrational zero-point level, resulting in a dip or decrease in the cold UV photofragment signal. By contrast, in IR gain spectroscopy, the UV laser is fixed off-resonance from any UV transitions of the cold ion. Since IR-excited molecules possess a broadened UV absorption spectrum, this broadened absorption can partially cancel the depletion signal on-resonance or can produce a gain signal when the UV is off-resonance. At the off-resonant UV wavelength, an IR gain spectrum is recorded by tuning the IR wavelength. These spectra are against zero background (ideally) but lack conformation specificity. When the IR gain and dip spectra match, it is a strong indication that only one conformer of the parent ion is present in the cryo-cooled cell.

III. COMPUTATIONAL METHODS

III.A. Conformational Minima and Energetics. We carried out conformational searches for the K^+-BzCrypt and Ba^{2+}-BzCrypt complexes based on molecular dynamics (MD) simulations using TINKER software[48] with the AMOEBA force field.[49] The automated parameterizing program POLTYPE2 was used to generate AMOEBA parameters for the BzCrypt, and the ion parameters were taken from amoeba-bio18.prm. We calculated the hydration free energy of Ba^{2+} in order to validate the Ba^{2+} parameters, obtaining a value of −295.96 kcal/mol, which is in close agreement with the experimental value (−296.60 kcal/mol, see the Supporting Information, SI).[50] The K^+ parameters were previously reported and validated.[51] Starting structures for the M^{+n}-BzCrypt MD simulations were provided by X-ray crystal structures for [2.2.2]benzocryptand (Kryptand 222B, PubChem) with the ions placed at the midpoint between the two capping nitrogens in the cryptand cage. We carried out simulations of the complexes at a high temperature (1000 K) for 50 ns[52] to search conformational space, with one structure frame saved every 5 ps. Each frame was then minimized using TINKER with the AMOEBA force field.

We grouped the ensemble of optimized structures into 20 closely similar "clusters" of structures using the K-means clustering algorithm of Lightweight Object-Oriented Structure-analysis (LOOS).[53] Representative frames from the clusters were taken as starting points for quantum mechanical (QM) structure optimization using Gaussian16 software.[54] We took the most similar frames instead of the generated cluster structures to ensure that the structures used for density functional theory (DFT) optimization were ones sampled by the MD simulation.[55,56] The DFT calculations employed the TPSSTPSS functional with mixed atomic basis sets that used cc-pVTZ for H (hydrogen), aug-cc-pVTZ for C (carbon), O

https://doi.org/10.1021/acs.jpca.3c03457
J. Phys. Chem. A 2023, 127, 6227−6240

(oxygen), and N (nitrogen), the MWB64 pseudopotential with associated basis set for Ba (barium), and a 6-311++G(2d,2p) basis set for K (potassium). This functional and these basis sets were chosen based on previous studies of similar ions.[51,57] The energies of these optimized structures were then compared to determine the lowest energy structure from each cluster. Based on this energy ordering, other members of the lowest energy structures from the groups were taken as starting structures for structure optimization. Binding energies for the assigned structures were computed at the same levels of theory, including corrections for both zero-point energy and basis set superposition error (BSSE).[48] In addition, we also optimized the lowest energy structure using B3LYP/6-311++G(d,p) and computed the binding energy at the same level of theory to compare different DFT methods.

As a final check for completeness, random searches were performed through dihedral angle space for each of the three strands looking for structures that satisfied reasonable N−N distances for ion contact and had reasonable O−C−C−O dihedrals to get metal ion bonding. The lowest energy structure from this search (called conformer A in what follows) is slightly lower than the lowest energy structure sampled from the MD cluster representatives (conformer B). These two lowest energy structures of K^+-BzCrypt (conformers A and B) are shown in Figure 2a,c, while conformer A in Ba^{2+}-BzCrypt is shown in Figure 2b for comparison. Conformer B was verified as a MD structure sampled in one of the clusters, which suggests that using cluster representative structures is not the most effective search method. This lowest energy structure and the MD sampled structures were combined to form a set of structures on which to carry out vibrational analysis.

III.B. Local Mode Anharmonic Model of the Alkyl CH Stretch Spectral Region. Our modeling of the CH stretch region for molecules containing CH_2 groups uses a localized representation of the molecular vibrations. In this representation, the only anharmonic coupling is between the two localized CH stretches and the overtone of the corresponding scissor vibration of individual CH_2 groups. If there are N CH_2 groups, then the 2N stretches of the different groups are all quadratically coupled to each other, as are the N scissor vibrations. This coupling is a result of the localization of the vibrations introducing quadratic bilinear coupling terms into the potential.

The Hamiltonian matrix used in our model is obtained in a two-step process. In the first step, one finds a harmonic localized matrix representation for the stretches and scissors, the eigenvalues of which are essentially the same as those of normal modes. The second step includes scaling the local harmonic frequencies and adding the abovementioned Fermi couplings. We briefly review these two steps below.

In our mode localization approach, as well as in others,[58−63] the local modes are obtained as an orthogonal transformation of a select set of normal coordinates. The details can be found that work.[60−65] We transform to localized normal coordinates $\mathbf{Q} = \mathbf{Aq}$, where $\mathbf{A}$ is an orthogonal matrix that is block-diagonal and $\mathbf{q}$ are the normal coordinates. One block of this matrix maps those $2N$ normal modes involving CH stretches onto $2N$ localized normal modes. The same is true for the N scissor vibrations. If the normal modes themselves are complex admixtures of stretches and bending modes, more sophisticated localization schemes need to be employed; however, this is not necessary in the present work. If a normal mode q_j is not among those modes that we chose to localize, then we leave it unchanged by setting $A_{kj} = \delta_{kj}$, where δ_{kj} is the Kronecker delta.

Local mode models offer simpler representations than normal modes for modeling anharmonicities. We have demonstrated that these models allow one to describe the CH stretch region of IR spectra with a few select anharmonic couplings between local modes sharing common atoms. Equally important, these couplings vary little from molecule to molecule, so they do not need to be recalculated for each molecule. The key Fermi coupling in our model is a 22 cm^{-1} Fermi coupling matrix element between a CH_2 scissor overtone and a contiguous CH stretch fundamental. Equally important to our model is the use of a scaling of the harmonic frequencies. It is well known that the harmonic frequencies obtained with density functional theory should be scaled when compared to experiment. Our work typically uses the harmonic scalings developed by Tabor et al.[41] that are specific for CH stretches (0.960) and CH_2 scissor (0.975) vibrations when one is working at the B3LYP/6-311++G(d,p) level of theory. These scalings are applied to the diagonal elements of the local mode Hamiltonian.

In our previous models of the CH stretch region, there were only a few instances in which coupling to modes other than the scissor degrees of freedom needed to be considered. In one study, we included couplings to the CH_2 wag in an instance where the CH stretch was significantly red-shifted, this being the case of the Li^+-cyclohexane complex.[64,65] In general, the wag overtones and combination bands are so low in energy that their Fermi coupling to the CH stretch fundamentals can be ignored. However, in the cryptand complexes, the wag normal mode frequencies extend up to 1460 cm^{-1}, as shown in the right-hand panel of Figure 2a, where B3LYP/6-311++G(d,p) level normal mode results are plotted for the CH_2 scissors and wags. For comparison, the corresponding local mode results are shown on the left-hand side of Figure 2a. Note that the local scissors and wag transitions are closely grouped around 1500 and 1410 cm^{-1}, respectively. These values can be compared to the analogous CH_2 scissor and wag vibrations in *trans* and *gauche* CD_3-CH_2-CH_2-CD_3, an all-alkyl chain. In that case, the two scissor transition energies are 1496/1496 cm^{-1} for *trans* and 1492/1492 cm^{-1} for the *gauche* conformer. Strikingly, the analogous wag transition energies are 1358 and 1375 cm^{-1}, respectively. Clearly, the wag local mode frequencies are much higher for the cryptand cage, where the CH_2 groups are adjacent to N- or O-atoms, than those of pure alkyl chains.

In addition to the higher local mode wag frequencies, there are important off-diagonal effects. Comparing the left and right columns of Figure 3a, one observes similar local and normal scissor frequencies. This similarity is a consequence of the weak coupling between the local scissor modes. In contrast, the local wags are strongly coupled to one another. It is this strong coupling that leads to the large spread in energies in the normal mode picture, which in turn leads to the wags being relevant for describing the CH stretch spectral region. Having established this fact, we now look at these couplings in more detail.

Figure 4 shows the coupling between the local wags along a strand of the K^+-BzCrypt complex for Conformer A. While there is a large coupling (>10 cm^{-1}) between each adjacent CH_2 group, the coupling between the second and third CH_2 wags (counting left to right) and again between the fourth and fifth is extraordinarily strong (~27 cm^{-1}). These pairs of CH_2

https://doi.org/10.1021/acs.jpca.3c03457
J. Phys. Chem. A 2023, 127, 6227−6240

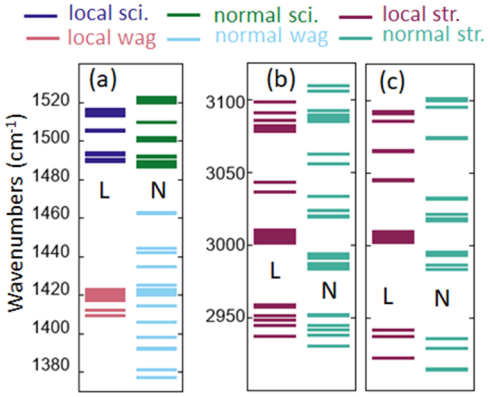

Figure 3. Local (L) and normal (N) mode transition energies of the K^+-BzCrypt complex for conformer A (a, b) and conformer B (c) for the CH_2 scissor and wag vibrations (a) and the CH stretch vibrations (b) and (c). Wag transition energies lie below 1464 cm^{-1}. Results are unscaled B3LYP/6-311++G(d,p) level results. Coupling between the local scissor states is weak, as seen by the similarity of the normal and local mode results. In contrast, the local wag energies are nearly degenerate and strongly coupled.

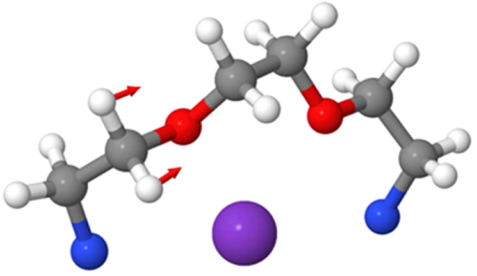

$$\mathbf{H}_A = \begin{pmatrix} 1418.34 & & & & & \\ 13.27 & 1418.20 & & & & \\ 1.69 & 27.65 & 1420.27 & & & \\ -2.00 & -1.60 & -18.26 & 1421.44 & & \\ -0.31 & 1.22 & 1.59 & -27.82 & 1419.16 & \\ -0.04 & 0.32 & -1.93 & 1.63 & -13.39 & 1422.09 \end{pmatrix}$$

Figure 4. Local mode CH_2 wag Hamiltonian for one of the alkyl ether chains of conformer A of the K^+-BzCrypt complex. The diagonal elements of the matrix correspond to the wag states with one quantum of excitation as one moves from left to right across the fragment that is shown. The local vibration, indicated with the red arrows, has a transition energy of 1418.20 cm^{-1} calculated at the B3LYP/6-311++G(d,p) level. Note the strong wag/wag coupling in the CH_2-O-CH_2 fragments.

groups are separated by an oxygen atom. For comparison, the scissor coupling between consecutive CH_2 groups is 0.8, 9.4, 0.2, 9.3, and 0.9 cm^{-1}.

It is the combination of higher wag local mode frequencies combined with large quadratic couplings that are responsible for the wag vibrations in the cryptand complex extending up to 1460 cm^{-1} in the B3LYP/6-311++G(d,p) calculations. In order to incorporate these modes into our model of the CH stretch vibrations in a comparable way to how we include the scissors, we need to explore the nature of the wags in more detail.

In this section, we describe the extension of our local mode model to include the CH_2 wag degree of freedom. At the harmonic level, this is relatively straightforward for these complexes, since there are 16 normal modes that can be described as linear combinations of CH_2 wags. However, the inclusion of anharmonic couplings requires an analysis that includes the CH_2 twisting modes as well as the wags. To illustrate the key ideas, we consider the local modes of a deuterated propane CD_3-CH_2-CD_3 molecule, focusing on the bending vibrations of the CH_2 group.

There are four normal mode CH_2 bending modes for this high-symmetry molecule: the rock, twist, wag, and scissor modes. In our previous work, these modes would also be considered local modes, since the vibrations are localized on a single CH_2 group. However, to appreciate the subtle differences between wags and scissor vibrations, we take the concept of localization one step further and localize the bends onto the individual CH groups. The two CH localized modes associated with the upper H-atom are shown in Figure 5. Panel

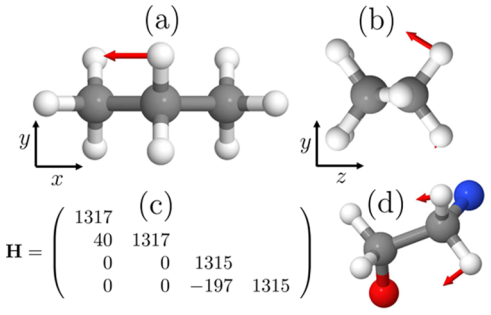

Figure 5. Panels (a) and (b) are two nearly degenerate CH bending local modes for butane CD_3-CH_2-CD_3. Panel (c) shows the lower diagonal of the corresponding local mode Hamiltonian with rows 1 and 3 corresponding to vibrations (a) and (b), respectively. Rows 2 and 4 correspond to analogous vibrations on lower H-atom of CH_2 group. Panel (d) shows a localized "wag" motion in which H-atoms have different amplitudes. Results obtained at the B3LYP/6-311++G(d,p) level of theory.

(a) shows the upper H moving parallel along the x-axis, and panel (b) shows H-atom motion in the y−z plane. These local vibrations have frequencies 1317 and 1315 cm^{-1}, respectively, at the B3LYP/6-311++G(d,p) level of theory.

The corresponding Hamiltonian matrix describing one quantum of excitation of these two vibrations is shown in Figure 5c, which also includes the two analogous vibrations for the lower H-atom. Here, the first two rows correspond to the upper and lower H-atom vibrations along the x-axis; the last two rows correspond to vibrations in the y−z plane. A noteworthy feature of this Hamiltonian is the large magnitude of the H_{43} = −197 cm^{-1} coupling. For most CH_2 environments, the differences between site energies H_{33} and H_{44} are small compared to the magnitude of this coupling. As a result, modes 3 and 4 strongly mix, leading to a low-frequency rock and a high-frequency scissor motion. In between these two sets of modes, we have the twists and wags. These modes are close in energy due to the smaller H_{21} coupling of 40 cm^{-1}. In the above coupling scenario, normal modes correspond to a higher energy, in-phase wag and a lower energy, out-of-phase twist vibration. Because of the high symmetry of this example, the mixing is 50:50; both the wag and twist vibrations correspond to motions for which the amplitude of the H-atoms are the same. However, the presence of a gauche kink in an alkyl chain such as g-butane CD_3-CH_2-CH_2-CD_3 leads to a difference in site energies H_{11} and H_{22}, with the result that the amplitude of motion of the two H-atoms is no longer the same. Figure 5d

https://doi.org/10.1021/acs.jpca.3c03457
J. Phys. Chem. A 2023, 127, 6227−6240

shows select atoms involved in a CH_2 localized wag motion of the A conformer of K^+-BzCrypt complex. The lower H-atom of the figure has a larger amplitude motion.

The goal of our work is to provide transferable anharmonic couplings, so that one can avoid the calculation of the many cubic terms associated with molecules of the size being considered herein. For the scissor modes, the Fermi couplings are nearly unchanged in size ($\sim$30 cm^{-1}) for all of the molecules we have studied to date. Based on the above analysis, we see that this similarity results from the strong coupling H_{43} described above. For this reason, we were able to assume a single-scaled Fermi coupling matrix element of 22 cm^{-1}, a value obtained empirically by fitting to select model systems.

In contrast, the wag shown in Figure 5d is expected to couple differently to the rightmost two CH stretches shown in the figure. One expects greater coupling to the CH stretch that has the larger red arrow attached to it. The simplest model would assume that this coupling scales quadratically with the length of the red arrows shown in the figure, where the arrows scale with the amplitude of the H-atom motion. In order to complete our model, we seek a means to predict the stretch-wag coupling without recourse to calculating cubic force constants explicitly for each individual situation.

Specifically, from our previously described localization procedure, we calculate $\mathbf{x} = \mathbf{lq} = \mathbf{lA}^T\mathbf{Q}$. Here, the $\mathbf{x}$ are the Cartesian coordinates, and $\mathbf{l}$ is obtained by diagonalization of the Hessian used in normal mode calculations. For a unit displacement of the localized wag normal mode Q_k, we calculate the corresponding displacements in the Cartesian coordinates. If $\mathbf{x}_H$ and $\mathbf{x}_C$ are the displacement vectors, respectively, of the H- and C-atoms of the localized wag, then the amplitude of the H-atom motion is given as $d = |\mathbf{x}_H - \mathbf{x}_C|$. Plotting the stretch-wag Fermi coupling, calculated using finite differences of *ab initio* single point calculations as a function of d^2, we obtain the results shown in Figure 5. We note that the squared dependence on "d" is a result of the coupling scaling quadratically with the wag coordinate. The quality of the fit is sufficiently good that we can use the results to predict the wag coupling from this best-fit result. Fits with the intercept constrained to zero are nearly as good, but we have chosen the more general form in our work for predicting couplings. If both H-atoms have similar displacements, the coupling is about 45 cm^{-1}. Just as was the case for the scissors, it is necessary to scale the *ab initio* values.

The results of Figure 6 allow us to infer the CH stretch/CH_2 wag coupling between all of the local modes of the M^{n+}-BzCrypt complexes, given the output of a normal mode calculation. The wag degrees of freedom are treated at the same level as the scissor modes, with the exception that the diagonal anharmonicity term that shifts the wag overtone transition energy from that of the combination bands is assumed to be zero.

IV. RESULTS AND ANALYSIS

IV.A. UV Photofragment Spectra. Figure 7 presents the UV photofragment spectra of K^+-BzCrypt and Ba^{2+}-BzCrypt over the 35,820−37,500 cm^{-1} region. The S_0-S_1 origin of K^+-BzCrypt is at 35,925 cm^{-1}, while that for Ba^{2+}-BzCrypt is shifted 521 cm^{-1} further to the blue, appearing at 36,446 cm^{-1}. Both UV photofragment spectra have a rather dense set of low-frequency vibronic activity and vibronic structure at higher frequency that reflect localized structural changes in the phenyl

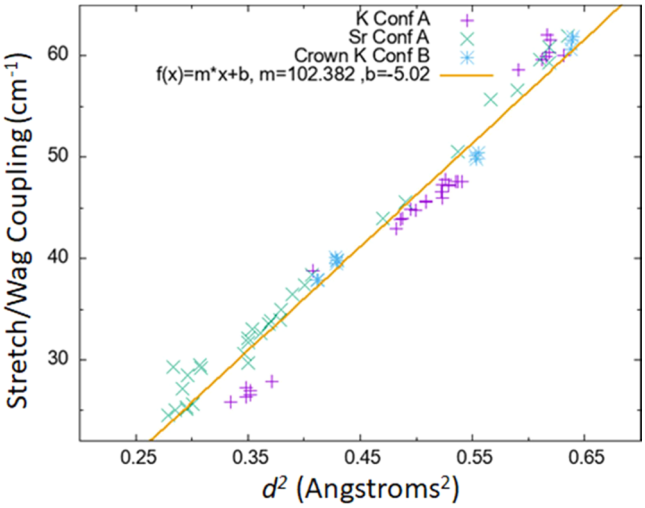

Figure 6. Plot of CH stretch/CH_2 wag Fermi coupling matrix elements obtained from B3LYP/6-311++G(d,p) level Gaussian calculations for conformers A of the K^+-BzCrypt, Sr^{2+}-BzCrypt, and a low energy conformer of the K^+-12-crown-4 complex[66] plotted as a function of d^2, the H-atom displacement squared. Also shown are the results of a linear least-squares fit.

ring upon $\pi\pi^*$ excitation, involving in-plane ring deformation (ν_{18}, ν_{15}) and ring breathing (ν_{17}) motions.

A close-up view of the first 300 cm^{-1} of the UV photofragment spectra is shown in Figure 8, highlighting the low-frequency vibronic activity that more directly probes the response of the confined ion to the electronic excitation of the cage.

Given the structure of benzocryptand (Figure 1b), a close structural analogue of its UV chromophore is 1,2-dimethoxybenzene (DMB), whose UV spectroscopy has been studied both in isolated neutral form[36] and when bound to alkali metal cations.[35] The S_0-S_1 origin of neutral DMB occurs at 35,751 cm^{-1}, so that the caged K^+ shifts the electronic origin 174 cm^{-1} to the blue relative to DMB. This shift is significant but much smaller than in K^+-DMB (>1000 cm^{-1}).[35] Furthermore, the electronic origin of K^+-BzCrypt is the most intense transition in the spectrum, while the electronic origin of K^+-DMB cannot be detected, as the UV absorption supports a long FC progression indicative of a large change in geometry between ground and excited states. We surmise on this basis that the cryptand cage, with its eight lone pairs contributing to the binding of the ion, both weakens the interaction of the ion with any single oxygen atom and confines the motion of the ion so that the electronic origin transition is dominant in the K^+-BzCrypt spectrum. In Ba^{2+}-BzCrypt, the S_0-S_1 origin is shifted 521 cm^{-1} to the blue of that in K^+-BzCrypt due to the stronger electron-withdrawing effect of the +2 cation on the two oxygens bound to the phenyl ring.

Mass spectra recorded at the S_0-S_1 origin transitions of K^+-BzCrypt showed major photofragments 28, 30, and 58 mass units below the parent ion (Figure S1), indicating that a segment of one of the bridges (C_2H_4, H_2CO, C_2H_4+H_2CO) is lost from the ion following UV excitation, rather than removing the ion from the cryptand cage. This is consistent with the strong binding energies anticipated for the ions to their cryptand cage.

IV.B. IR−UV Gain and Dip Spectra. Given the sharp, strong S_0-S_1 origin transitions of K^+-BzCrypt and Ba^{2+}-

https://doi.org/10.1021/acs.jpca.3c03457
J. Phys. Chem. A 2023, 127, 6227−6240

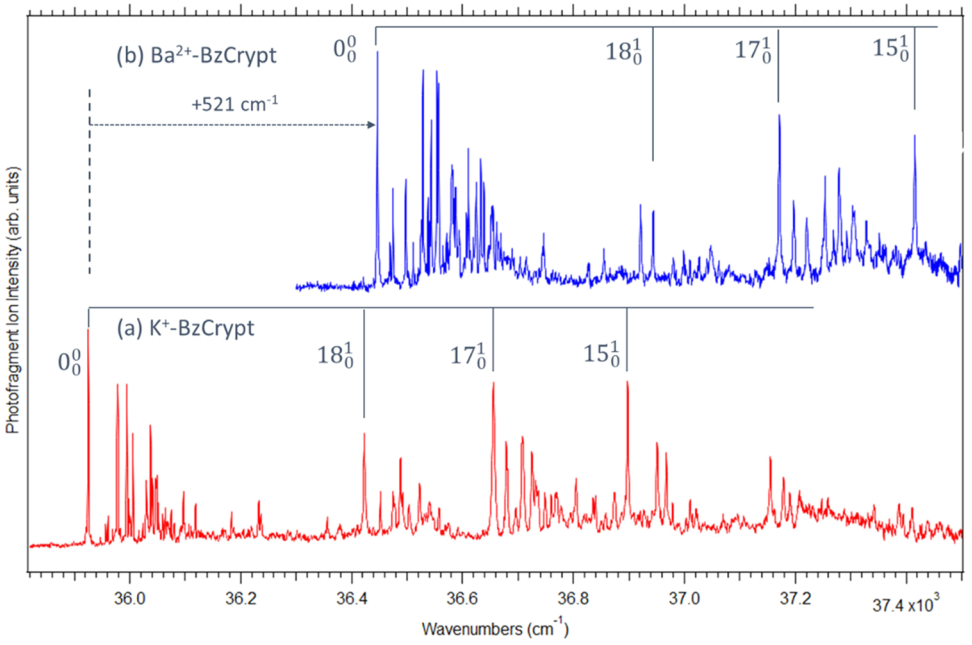

Figure 7. Overview UV photofragment spectra of (a) K^+-BzCrypt and (b) Ba^{2+}-BzCrypt complexes in the region of their S_0-S_1 transitions. Tentative assignments are given for the vibronic transitions using the notation in Tuttle et al.[67] appropriate for ground-state vibrations in ortho-disubstituted benzenes.

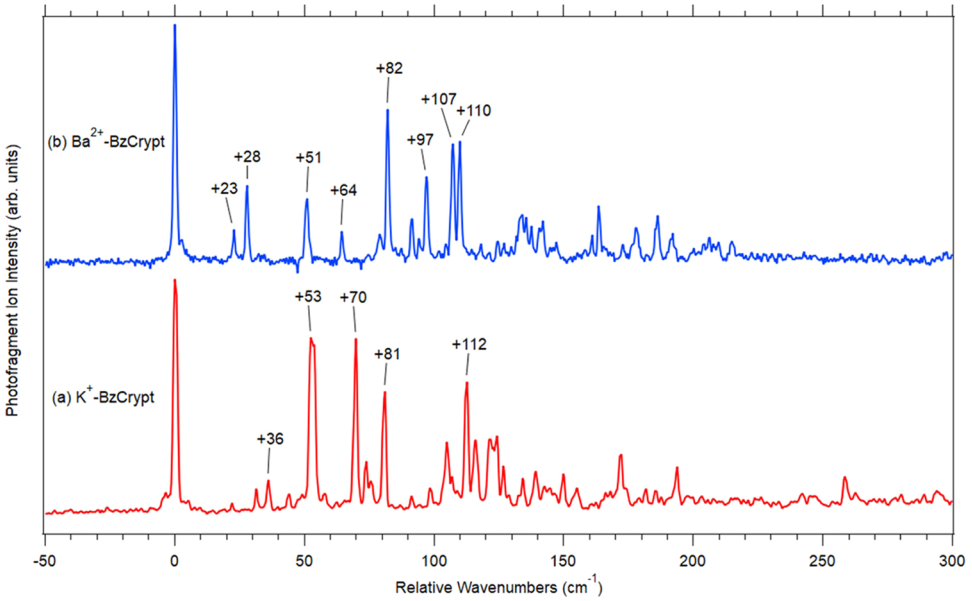

Figure 8. Close-up view of the first 300 cm^{-1} of the (a) K^+-BzCrypt and (b) Ba^{2+}-BzCrypt S_0-S_1 UV photofragment spectra on a relative wavenumber scale. The absolute frequencies of the two electronic origins are (a) 35,925 cm^{-1} and (b) 36,446 cm^{-1}, respectively.

BzCrypt, we used these UV absorption wavelengths to record conformer-specific infrared spectra using IR−UV dip spectroscopy. An overview spectrum of K^+-BzCrypt over the 2300−3800 cm^{-1} region (Figure S2) shows absorptions only in the alkyl CH stretch region (2800−3000 cm^{-1}), with a very weak aromatic CH stretch transition appearing at 3080 cm^{-1}. A close-up view of the alkyl CH stretch region is shown in Figure 9b, where it is compared with an IR−UV gain spectrum (Figure 9a) recorded with the UV laser fixed at 35,870 cm^{-1}, just to the red of the S_0-S_1 origin. The close correspondence between the two spectra indicates that there is a single dominant conformation of K^+-BzCrypt, so that only absorptions due to this single conformer contribute to the gain spectrum, which is not conformer-specific. The analogous IR−UV dip spectrum of Ba^{2+}-BzCrypt, shown in Figure 9c, is surprisingly different from that of K^+-BzCrypt, most notably in having the lower-frequency portion of the spectrum shifted to higher wavenumber. The corresponding gain spectrum at the UV conditions used in Figure 9c was very weak.

IV.C. Conformational Landscapes. The conformational landscapes for K^+-BzCrypt and Ba^{2+}-BzCrypt are constrained by the bimacrocyclic cryptand structure itself and the overwhelming preference of the ions to imbed themselves inside the three-dimensional cage. As a result, one can categorize the low-lying energy conformers by the dihedral angles of each of the three linking chains of the cage (Tables

https://doi.org/10.1021/acs.jpca.3c03457
J. Phys. Chem. A 2023, 127, 6227−6240

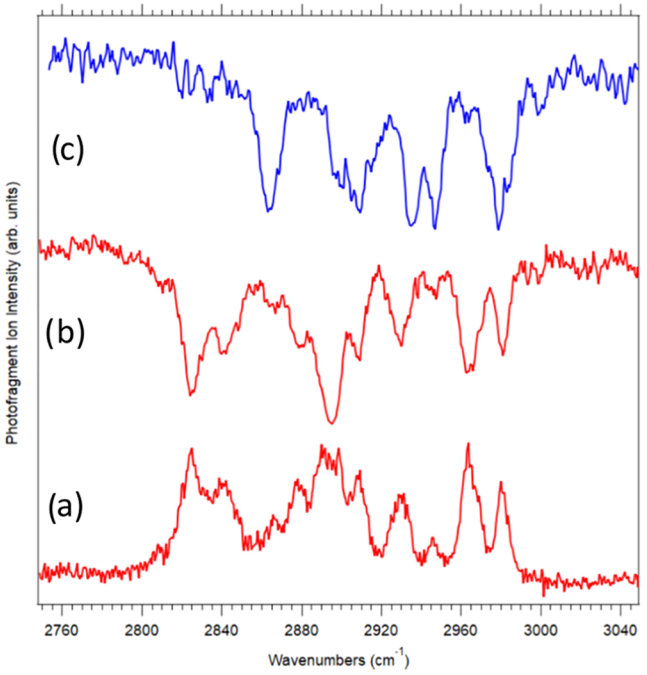

Figure 9. Comparison of the (a) IR−UV gain and (b) IR−UV dip spectra of K^+-BzCrypt, with UV fixed on the S_0-S_1 origin at 35925 cm^{-1}. The correspondence between the two spectra demonstrates that there is a single dominant conformer of this complex. (c) IR−UV dip spectrum of Ba^{2+}-BzCrypt with UV fixed on the S_0-S_1 origin at 36446 cm^{-1}.

S1 and S2). In both complexes, there are two structures, labeled A and B, that are significantly lower in energy than others, with A below B by almost 1000 cm^{-1} (2.9 kcal/mol) lower in energy than B, including zero-point energy correction, while in Ba^{2+}-BzCrypt, this difference shrinks to 425 cm^{-1} (1.2 kcal/mol). Two views of the global minimum structures of K^+-BzCrypt and Ba^{2+}-BzCrypt (conformer A) are shown in Figure 2a,b respectively, while the analogous views of its main energetic competitor, conformer B, are shown in (Figure 2c). Calculated relative energies for the sixteen lowest energy conformers of K^+-BzCrypt are summarized in Table 1, while the analogous results for Ba^{2+}-BzCrypt are in Table S3, which also includes a more detailed comparison of the relative energies as a function of the level of theory, given that Ba^{2+}, as a 6th-row element, necessitates incorporation of an effective core potential. Structures for the eight lowest energy structures of the K^+/Ba^{2+}-BzCrypt complexes are shown in Figures S3 and S4, respectively, all of which are embedded ion structures. Local minima that incorporate cation−π interactions, while potentially present, are far less stable than the embedded ion structures.

IV.D. Modeling and Structural Assignment. Based on the results of the conformational search, we calculated the alkyl CH stretch spectra for the 16 lowest energy conformers of both K^+-BzCrypt and Ba^{2+}-BzCrypt using the local anharmonic model, including both stretch-scissors and stretch-wag anharmonic coupling terms. Fine-tuning of the CH fundamental scale factor and stretch-wag Fermi coupling led to finalized values that were used in all subsequent modeling (Figures S6 and S7). The calculated CH stretch spectra for K^+-BzCrypt are compared in Figure S8, which demonstrates the sensitivity of the alkyl CH stretch region to the cage conformation.

Table 1. Relative Energies ΔE_o and Zero-Point Corrected Energies ΔE_{zpe} in cm^{-1} for the K^+-Cryptand Complexes Calculated at the B3LYP/6-311++g(d,p) Level

structure	ΔE_o	ΔE_{zpe}
A	0.0	0.0
B	868.6	989.6
C	1185.1	1163.7
D	1069.6	1003.7
E	1525.4	1498.6
F	2084.6	2216.3
G	2286.7	2295.3
H	1241.3	1335.7
I	1848.0	1760.8
J	1866.1	1734.9
K	1353.7	1427.2
L	3010.2	3090.9
M	1825.0	1929.4
N	2867.2	2843.3
O	1686.5	1668.2
P	1727.5	1780.8

Figure 10a compares the calculated spectra for structures A and B of K^+-BzCrypt to experiment, while the analogous results for Ba^{2+}-BzCrypt are shown in Figure 10b. In the K^+-BzCrypt complex, structure A provides an excellent fit to the spectrum, significantly better than that of conformer B or any other of the calculated spectra (Figure S8), leading to an unambiguous assignment of the experimental structure to conformer A (Figure 9a). On the other hand, the calculated spectra for structures A and B in Ba^{2+}-BzCrypt are not as obviously different. While the fit is somewhat better for A than B, the smaller energy difference prevents a completely firm assignment. In what follows, we focus our primary attention on structure A of both complexes.

V. DISCUSSION

V.A. Structural Analysis. One of the motivations for comparing the structures and spectroscopic signatures of K^+- and Ba^{2+}-BzCrypt is that the ionic radii of K^+ (152 pm) and Ba^{2+} (149 pm) are nearly identical, while the charge differs by a factor of two, providing a clean comparison of the effect of charge on the structure and spectroscopy of the caged ion complex.[33] Furthermore, [2.2.2]cryptand is known to selectively bind K^+ and Ba^{2+} over other alkali and alkaline earth cations in aqueous solution.[34]

Consistent with this similarity in size, the structures assigned to K^+-BzCrypt and Ba^{2+}-BzCrypt are strikingly similar (Figure 2a,b). There are several features to be noted. First, the assigned structures for the K^+-BzCrypt and Ba^{2+}-BzCrypt complexes have six oxygen atoms forming the primary binding sites for the cations ($M^{+n}\cdots O$ of ∼2.80 Å), while the two capping nitrogen atoms reside in secondary binding positions about 0.2 Å further away. These calculated distances are very close to those from the X-ray structures for the corresponding K^+/Ba^{2+}-[2.2.2]cryptand, which lack the phenyl ring and experience solid-state packing interactions.[5] This close similarity is a testimony to the robust and stable geometry of the cryptand cage when imbedding K^+ or Ba^{2+} inside it.

Second, the two alkyl ether chains take up alternating g+/g-/g+ conformations about the N−C−C−O/O−C−C−O/O−C−C−N dihedrals (Tables S1 and S2), while the aromatic ring forces an eclipsed geometry for the central O−C(ph)−

https://doi.org/10.1021/acs.jpca.3c03457
J. Phys. Chem. A 2023, 127, 6227−6240

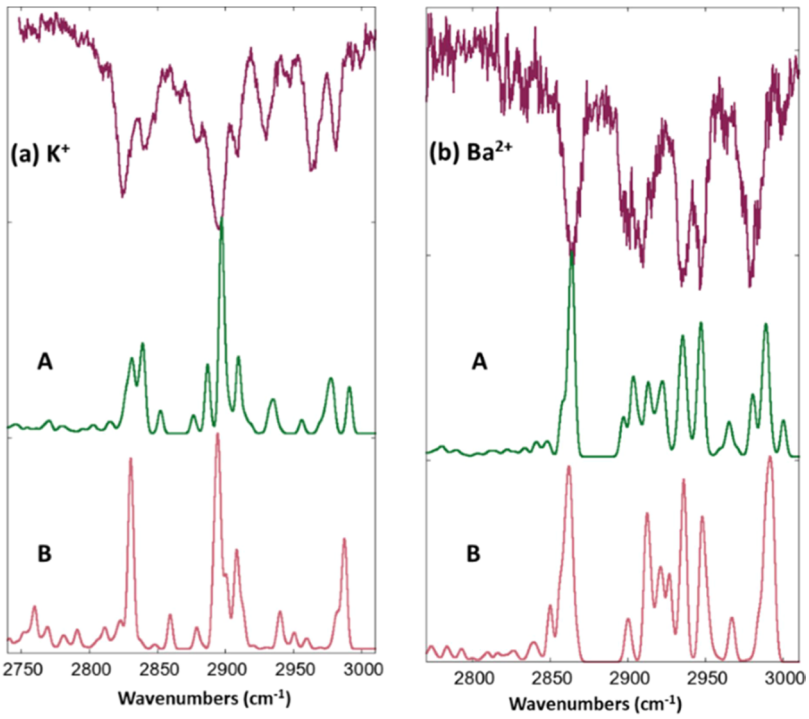

Figure 10. Experimental IR−UV dip spectra compared to theoretical predictions for conformers A and B of (a) K^+-BzCrypt and (b) Ba^{2+}-BzCrypt cage complexes. See text for further discussion.

C(ph)−O leg of its bridge (g+/e/g+). Third, in the global minimum structure A, the phenyl ring bends toward one of the other alkyl ether bridges about 65° away from vertical, as highlighted by the end-on view of the structure in Figure 2. This asymmetry in phenyl ring orientation is produced by an asymmetry in the two C(ph)−O−C(alk)−C(alk) dihdedrals of 176/92° in K^+-BzCrypt and 174/125° in the Ba^{2+}-BzCrypt complexes. Finally, the relative orientation of the N−C bonds of the two capping tertiary amines is significantly different. Looking end-on, we see that these two triads of N−C bonds are nearly eclipsed in K^+-BzCrypt, with a C−N−N−C dihedral of 16°, while in Ba^{2+}-BzCrypt, this dihedral opens to 32°.

The distortion placed on the cage by the phenyl ring begs the question as to whether there is a more symmetric structure that can be formed. Early in our search process, we found just such a structure (Conformer B, Figure 2c) and initially identified it as the global minimum, only to be displaced later by the structures shown in Figure 2, which are even lower in energy. Conformer B has equivalent C(ph)-O-C(alk)-C(alk) dihedrals (156/156° in K^+ and 160/161° in Ba^{2+}), keeping the phenyl ring in-plane with the rest of its bridge backbone (the vertical plane in Figure 2c).

Computed binding energies of K^+ and Ba^{2+} to the benzocryptand cage, including corrections for zero-point energy and basis set superposition error (BSSE),[48] are strikingly large (72 and 209 kcal/mol, respectively) due to the interaction of the ion with lone pairs on six oxygen atoms and two nitrogen atoms. Second, the binding energies vary super-linearly with charge, with the Ba^{2+}-BzCrypt binding energy nearly three times that of K^+-BzCrypt. This difference in binding energies must be attributed to a combination of the magnitude of the charge and the subtle molecular structure differences between the two complexes. While the accepted ionic radii of K^+ and Ba^{2+} are quite similar, the average Ba^{2+}−O distance in the benzocryptand complex (2.80 Å) at the same level of theory is always slightly smaller (<0.1 Å) than in K^+-BzCrypt. Even such a small contraction in the cage may produce large changes to the binding energy.

V.B. Spectroscopic Signatures of Ion Binding to the BzCrypt Cage. By incorporating a UV chromophore into the cryptand cage, we are afforded a look at how binding K^+ and Ba^{2+} inside the cage affects the S_0−S_1 spectroscopy of this UV chromophore. As noted already, we use 1,2-dimethoxybenzene (DMB) as the reference UV chromophore for benzocryptand, since the UV spectroscopy of DMB has been studied in the gas phase previously.[36] Binding of a cation to the two DMB oxygen atoms produces a blue shift in the S_0−S_1 origin of +174 cm^{-1} in K^+-BzCrypt relative to DMB, but this blue shift increases to 695 cm^{-1} in Ba^{2+}-BzCrypt. Given the nearly identical M^{+n}···O distances in the K^+ and Ba^{2+} inclusion complexes, this increased blue shift is the response of the DMB chromophore in the BzCrypt cage to its ionic contents.

The magnitude of this shift represents the difference in binding energies between the ground and first excited singlet states, with a blue shift signifying that the excited-state complex is less strongly bound than the ground state by the magnitude of this shift. The recent study of the S_1 state structure of 1,2-DMB[68] deduced an increased quinoidal structure in the S_1 state arising from increased participation by resonance structures that increase the double bond character of the C−O bonds, with an accompanying positive charge on the oxygen atoms. In the presence of a cation bonded to these oxygens, we anticipate a weaker binding energy in the excited state, as observed. This is consistent with the study of the cryo-cooled, gas-phase K^+-DMB complex by Inokuchi et al.,[35] who observed a Franck−Condon maximum at a shift of >1000 cm^{-1} to the blue of the monomer. By comparison, the K^+-BzCrypt cage, in which the cation charge is shared between six oxygen atoms, produces an electrostatic environment with a much smaller shift (+174 cm^{-1}) than the bare K^+ cation. The decrease in

https://doi.org/10.1021/acs.jpca.3c03457
J. Phys. Chem. A 2023, 127, 6227−6240

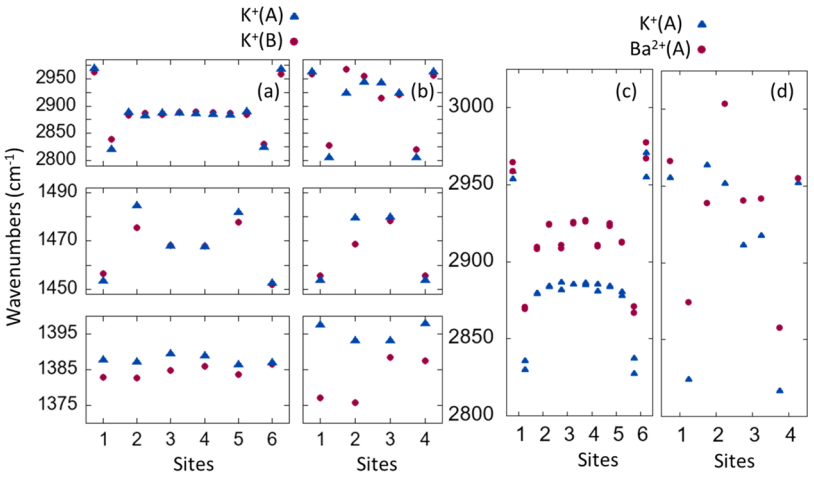

Figure 11. (a, b) Scaled site frequencies (cm^{-1}) for an −Et−O−Et−O−Et− chain (a) and −Et−O−Ph−O−Et− chain (b) for the CH stretches (top), CH_2 scissors (middle), and wags (bottom) of K^+-BzCrypt conformers A (red) and B (blue), based on calculations carried out at the DFT B3LYP/6-311++G(d,p) level of theory. The CH stretch local modes are scaled by 0.9589, while the scissor and wag frequencies are scaled by 0.975 and 0.980, respectively. (c,d): Corresponding comparison of the uncoupled CH stretch local mode frequencies of conformer A complexes of K^+-BzCrypt and Ba^{2+}-BzCrypt.

electron density available for binding to the cation results in a much larger blue shift in Ba^{2+}-BzCrypt (+695 cm^{-1}).

The infrared spectra in the alkyl CH stretch region are also unique to whether K^+ or Ba^{2+} is imbedded inside the cage and to the conformation of the cage itself. This sensitivity of the CH stretch region is somewhat surprising, since the CH_2 groups are not directly interacting with the ion but rather are responding to the binding of the ion to the O- and N-atoms in the cage. One of the strengths of the local mode anharmonic model implemented here is that it enables a deeper understanding of the contributions to the spectrum once it has been tested against experiment. Given the model's quantitatively accurate description of the observed IR spectra, we focus here on the various contributions that produce the diagnostic frequency/intensity patterns that lead to the distinct differences between the alkyl CH stretch spectra of the K^+- and Ba^{2+}-BzCrypt complexes.

A starting point for such a discussion is simply to understand the local mode site frequencies of each of the CH groups in the M^{n+}-BzCrypt cages in the absence of any coupling. Figure 11a,b presents these scaled site frequencies (in cm^{-1}) for the CH stretch, scissors, and wag vibrational modes of conformers A and B of K^+-BzCrypt as a function of position in the cage structure. The panels in (a) are for a single alkyl ether chain, while those in (b) are for the phenyl-containing chain. Site numbers increase sequentially along each chain moving between the two N end groups. Each ethyl group has two carbon sites, so there are two CH energies for each site.

Consistent with Figure 3a, the site frequencies for the CH_2 scissors (middle) are spread over a range (~30 cm^{-1}) that is about 10 times greater than the spread in the wag frequencies (bottom, ~3 cm^{-1}). Figure 11 extends the results by showing how the site energies vary along the chain, with sites 1 and 6 in panel (a) and 1 and 4 in panel (b) showing notable shifts. These are the sites adjacent to the two capping N-atoms. These N-adjacent sites possess both the highest and lowest CH stretch transition energies, differing from one another by more than 130 cm^{-1}. These CH stretches dominate the high- and low-frequency regions of the CH stretch spectrum, since no other CH_2 groups contribute there.

The lone pair of electrons on the nitrogen atoms have an interesting role in these large splittings. Relative to the carbon backbone of the chain, the equatorial CH is the highest in frequency, while the axial CH, which is nearly antiparallel to the N···M^{+n} axis, is the lowest. This shift is even more pronounced in the $N(CH_3)_3$ molecule and is similar to that of methylamine, CH_3NH_2. For these molecules, it is the CH that is antiperiplanar to the nitrogen lone pair that has a lower frequency. These lower-frequency bands are known as Bohlmann bands, and the origin of the low-frequency CH stretch band in CH_3NH_2 has been discussed by Wolfe et al.[69] as being a destabilization that occurs as a result of charge transfer from the lone pair on the nitrogen atom to the π^* orbitals of the carbon atom. The presence of the M^{+n} ion diminishes this destabilization, leading to smaller CH downward shifts for the axial CH stretch band of the Ba^{2+} complex than that found for the K^+ complex. We note that the destabilization for the CH_3NH_2 molecule has also been elucidated by Glendening and Weinhold in terms of the effective weights of resonance structures calculated using natural resonance theory.[70]

In contrast, the site energies for the CH_2 groups adjacent to O-atoms are nearly degenerate. Since conformers A and B differ mostly in the orientation of the phenyl ring, it is not surprising that the largest difference between them is in the phenyl-containing chain, while the alkyl ether chains are nearly identical. This produces the differences between the two spectra that lead to the assignment of the observed spectrum to K^+-BzCrypt(A).

Figure 11c,d compares the site frequencies of the local CH stretch modes in K^+-BzCrypt (blue) with those in Ba^{2+}-BzCrypt (maroon). Note first that the local mode frequencies in the Ba^{2+}-embedded cage are all blue-shifted from those in K^+. This is a direct effect of the larger ion charge in the Ba^{2+}-BzCrypt complex relative to K^+-BzCrypt. Second, the blue shift in Ba^{2+} over K^+ is greatest in the axial CH groups adjacent to the N-atoms (sites 1 and 6), which are calculated to be near 2830 cm^{-1} in K^+, but at ~2865 cm^{-1} in Ba^{2+}. This accounts for the largest spectral difference observed between the two experimental spectra of Figure 10, where no transitions are

https://doi.org/10.1021/acs.jpca.3c03457
J. Phys. Chem. A 2023, 127, 6227−6240

observed below ~2850 cm^{-1} for Ba^{2+}-BzCrypt, while two strong transitions are present in K^+-BzCrypt. Figure S9 visualizes these wavenumber shifts in an energy level diagram contrasting Ba^{2+}-BzCrypt, K^+-BzCrypt, and neutral BzCrypt. Compared to neutral BzCrypt, the N-adjacent CH_2 frequencies in K^+/Ba^{2+}-BzCrypt are about 50/100 cm^{-1} higher in frequency. It is interesting that the most distinct difference in the spectra is due to the CH_2 groups next to the N, since the N-atoms are "second shell" binding sites to the cations. We see that the +2 charge on Ba draws electron density away from the N lone pairs much more effectively than K^{+1}. As discussed above, this electrostatic effect is transmitted most directly to the CH groups pointing away from the N lone pairs.

Finally, while Figure 10 compares the experimental IR−UV dip spectra with the results of the full theoretical model for the alkyl CH stretch region, in Figure 12, we show the effects of turning off specific coupling terms of the CH stretch fundamentals to the overtones of the scissors and wags. We use the results for conformer A of K^+-BzCrypt from the model, as this is the assigned structure for the experimental spectrum shown above it.

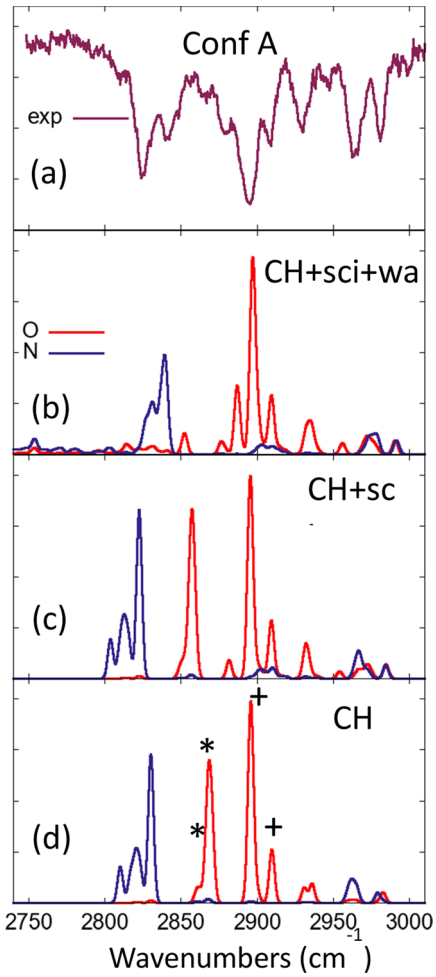

Figure 12. (a) Experimental IR spectrum of K^+-BzCrypt in the alkyl CH stretch region. (b)−(d) Results of the anharmonic local mode model of the CH stretch region, including only the CH stretch modes (d) (equivalent to the normal mode picture), the CH stretch + scissors couplings (c), and the full anharmonic model, including both scissors and wag couplings. Results of the model when the dipoles only from the CH_2 groups adjacent to the nitrogen (blue) or adjacent to O-atoms (red) are included. The total spectrum is the sum of red and blue. The transitions marked with asterisks (*) and pluses (+) are predominantly due to the alkyl ether CH_2 groups, with symmetric stretch/antisymmetric stretch split by about 40 cm^{-1}.

There are two spectra in each panel that serve to distinguish the CH spectral contributions of the K^+-BzCrypt complex. In Figure 12b−d, the eigenstates of the local mode Hamiltonian are the same, but the blue and red traces show the spectral contributions due to dipoles on the CH_2 groups adjacent to the nitrogens and oxygens, respectively. The plots of the dipole contributions show that the strong CH stretch transitions marked with an asterisk (*) and plus (+) in Figure 12d are predominantly due to the CH stretches of $O-CH_2-CH_2-O$ portion of the chain. These four CH stretches are nearly degenerate (Figure 11c) and therefore all couple to each other. The largest coupling (~−20 cm^{-1}) occurs between the two CH stretches on the same CH_2 groups. This coupling leads to symmetric stretch states (marked with asterisks in Figure 12d) about 40 cm^{-1} lower energy than their antisymmetric counterparts (marked with a +). When only the pure CH stretch modes are considered (Figure 12d), these four transitions dominate the central region of the spectrum, at odds with experiment. Furthermore, when the overtones of the scissors modes are included (Figure 12c), this qualitative result still holds, preventing an accurate fit to experiment. The scissors modes have so little effect because their overtones are shifted well to the blue of the CH stretch fundamentals carrying the main oscillator strength.

The results of coupling with the wags (Figure 12b) have two important effects, both of which greatly improve the agreement with experiment. First, the lower-frequency member of the CH stretch transitions due to the axial CH adjacent to the N-atoms are shifted to a higher frequency when the wag coupling is included. Second, the symmetric CH stretches of the $O-CH_2-CH_2-O$ fragment (*) are strongly mixed with wag overtones, leading to splittings that spread the CH stretch oscillator strength over several transitions.

VI. CONCLUSIONS

In this work, we have determined the gas-phase structures of K^+ and Ba^{2+} inclusion complexes with the [2.2.2]-benzocryptand cage using a combination of cryo-cooled ion spectroscopy and theoretical modeling. UV photofragment spectra and IR−UV double resonance spectra have provided the UV and IR spectroscopic signatures of these structures, proving that the ions are embedded in a single dominant conformation of the cryptand cage. As anticipated, the cations are bound to the cage principally through the six oxygen atoms and secondarily to the two nitrogens that are about 0.1−0.2 Å further away. The cryptand cage thus produces a ligand field for the ion made up of trigonal-prismatic oxygens capped at its two triangular faces by two N's. The ether chains thus largely retain the 3-fold symmetry arising from the capping tertiary nitrogens, but the phenyl ring breaks this symmetry by incorporating an eclipsed geometry at the O−C(ph)−C(ph)−O dihedral into an otherwise (g+, g−, g+) alkyl ether chain.

The strong interactions of the ion with the cage cause large blue shifts in the UV absorption frequency in the S_0-S_1 region of the benzocryptand chromophore that reflect a weakening of binding induced by electronic excitation of the phenyl ring. This weaker binding results from the quinoidal structure induced by $\pi\pi^*$ excitation of 1,2-dimethoxybenzene UV chromophore. The magnitude of the blue shift scales

https://doi.org/10.1021/acs.jpca.3c03457
J. Phys. Chem. A 2023, 127, 6227−6240

approximately with the magnitude of the S_0 binding energy. Future studies on a wider variety of M^{+n}-BzCrypt complexes would be useful to see whether this scaling is more generally true.

The strong binding of K^+ and Ba^{2+} inside the benzocryptand cage also leaves obvious signatures of its presence on the alkyl CH stretch IR spectra. In order to interpret these signatures, we needed to further develop the local mode anharmonic model of the alkyl CH stretch region. It is rather remarkable that the CH_2 groups that are themselves not directly involved in the binding to the ion nevertheless report sensitively on the ion binding to the O- and N-atoms, which engage in direct binding and transmit their perturbations to the CH_2 groups. Fermi resonance between the alkyl CH stretch fundamentals and the overtones of the CH_2 wags produce significant shifts and splitting in the spectra, with larger observable consequences than the CH_2 scissors, which are typically the anharmonic couplings of greatest importance. The strong inter-wag coupling across the ether oxygens and, to some degree, the capping nitrogens, produces a suite of strongly coupled CH_2 wag vibrations that envelop the cage, which differ in the relative phases of the localized CH_2 wag motions. As a result, the CH_2 wag fundamentals are spread over an exceedingly wide range (1346−1431 cm^{-1}), bringing the high-frequency members into 2:1 Fermi resonance with the CH stretch fundamentals, particularly in the 2800−2900 cm^{-1} region. Furthermore, the CH stretch region of the cryptand cage reports whether it is K^+ or Ba^{2+} that is bound inside it most noticeably through changes to the local mode frequency of the axial CH bonds on the N-adjacent CH_2 groups, which are shifted to a much higher frequency when interacting with Ba^{2+} than with K^+.

Taken as a whole, we conclude that both the electronic and vibrational spectra of the [2.2.2]-benzocryptand cage are sensitive probes of the cage's ionic contents, motivating further work that changes the nature of the embedded ion and/or the cage itself to explore these molecular-scale confinement effects. Extending the IR studies into the mid-infrared will also access the C−O stretches of the cage, which hold promise as direct reports of the ion coordination environment inside the cage.

■ ASSOCIATED CONTENT

Supporting Information

The Supporting Information is available free of charge at https://pubs.acs.org/doi/10.1021/acs.jpca.3c03457.

> Tables with the dihedral angles of 16 energetically low-lying conformers for both the K^+- and Ba^{2+}-BzCrypt complexes; figures showing photofragment mass spectra and an overview IR−UV depletion spectrum of K^+-BzCrypt; figures showing the structures of a subset of these conformers; figures showing the sensitivity of CH stretch spectral predictions to scaling factors for the CH_2 wag frequency and the CH stretch/wag Fermi coupling; a comparison of the CH stretch spectral results for 16 energetically low-lying conformers of the K^+-BzCrypt complex; an xyz file for conformer A of K^+-BzCrypt calculated at the B3LYP/6-311++G(d,p) is provided; and xyz files for other structures are available from the authors upon request (PDF)

■ AUTHOR INFORMATION

Corresponding Authors

Edwin L. Sibert, III − *Department of Chemistry, University of Wisconsin-Madison, Madison, Wisconsin 53706, United States*; Email: elsibert@wisc.edu

Timothy S. Zwier − *Gas Phase Chemical Physics, Sandia National Laboratories, Livermore, California 94550, United States*; orcid.org/0000-0002-4468-5748; Email: tszwier@sandia.gov

Authors

Casey D. Foley − *Gas Phase Chemical Physics, Sandia National Laboratories, Livermore, California 94550, United States*; Present Address: Department of Chemistry, University of Missouri, Columbia, Missouri 65211, United States; orcid.org/0000-0002-8828-8808

Cole D. Allen − *Department of Biomedical Engineering, University of Texas-Austin, Austin, Texas 78712, United States*

Kendrew Au − *Gas Phase Chemical Physics, Sandia National Laboratories, Livermore, California 94550, United States*

Chin Lee − *Gas Phase Chemical Physics, Sandia National Laboratories, Livermore, California 94550, United States*; orcid.org/0000-0001-9011-0526

Susan B. Rempe − *Center for Integrated Nanotechnologies, Sandia National Laboratories, Albuquerque, New Mexico 87185, United States*; orcid.org/0000-0003-1623-2108

Pengyu Ren − *Department of Biomedical Engineering, University of Texas-Austin, Austin, Texas 78712, United States*

Complete contact information is available at: https://pubs.acs.org/10.1021/acs.jpca.3c03457

Notes

The authors declare no competing financial interest.

■ ACKNOWLEDGMENTS

This work was suppSorted by the Laboratory Directed Research and Development program at Sandia National Laboratories, a multimission laboratory managed and operated by National Technology and Engineering Solutions of Sandia LLC, a wholly owned subsidiary of Honeywell International Inc. for the U.S. Department of Energy's National Nuclear Security Administration under contract DE-NA0003525. C.D.A. and P.R. acknowledge support for this work from a Sandia Academic Alliance Grant 21-0149 (contract agreement number 1885207). Calculations were performed, in part, at the Center for Integrated Nanotechnologies, an Office of Science User Facility operated for the U.S. Department of Energy (DOE) Office of Science. The views expressed in the article do not necessarily represent the views of the U.S. DOE or the United States Government. E.L.S. gratefully acknowledges support from NSF via Grant No. CHE-1900095.

■ REFERENCES

(1) Kang, S. O.; Llinares, J. M.; Day, V. W.; Bowman-James, K. Cryptand-like anion receptors. *Chem. Soc. Rev.* **2010**, *39*, 3980−4003.
(2) Schneider, H. J.; Yatsimirsky, A. K. Selectivity in supramolecular host-guest complexes. *Chem. Soc. Rev.* **2008**, *37*, 263−277.
(3) McKee, V.; Nelson, J.; Town, R. M. Caged oxoanions. *Chem. Soc. Rev.* **2003**, *32*, 309−325.
(4) Grommet, A. B.; Feller, M.; Klajn, R. Chemical reactivity under nanoconfinement. *Nat. Nanotechnol.* **2020**, *15*, 256−271.

(5) Chekhlov, A. N. Syntheses and Crystal Structures of (2.2.2-Cryptand)potassium Chloride and (2.2.2-Cryptand)ammonium Bromide((0.75))chloride((0.25)) Hydrates. *Russ. J. Inorg. Chem.* **2009**, *54*, 280−286.
(6) Metz, B.; Moras, D.; Weiss, R. Crystal Structures of 2 Barium Cryptates. *J. Am. Chem. Soc.* **1971**, *93*, 1806.
(7) Metz, B.; Moras, D.; Weiss, R. Crystal Structures of 3 Alkali-Metal Complexes with a Macrobicyclic Ligand. *J. Chem. Soc. D, Chem. Commun.* **1971**, *9*, 444.
(8) Metz, B.; Moras, D.; Weiss, R. A Crystal Structure of a Rubidium Cryptate Rb-C18H36N2O6-SCN-H2O. *J. Chem. Soc. D, Chem. Commun.* **1970**, *4*, 218.
(9) Metz, B.; Moras, D.; Weiss, R. Coordination of Earth Alkaline Cations in their Complexes with Macrobicyclic Molecules. 1. Crystalline and Molecular Structures of Calcium Cryptate C18H36N206.CaBr2-H2O. *Acta Crystallogr., Sect. B: Struct. Sci.* **1973**, *29*, 1377−1381.
(10) Metz, B.; Moras, D.; Weiss, R. Coordination of Earth Alkaline Cations in their Complexes with Macrobicyclic Molecules. 2. Crystalline and Molecular Structures of Barium Cryptate: C18H36N2O6.Ba(SCN)2-H2O. *Acta Crystallogr., Sect. B: Struct. Sci.* **1973**, *29*, 1382−1387.
(11) Metz, B.; Moras, D.; Weiss, R. Coordination of Earth Alkaline Cations in their Complexes with Macrobicyclic Molecules. 3. Crystalline and Molecular Structures of Barium Cryptate, C20H40N2O7.Ba(SCN)2.2H2O. *Acta Crystallogr., Sect. B: Struct. Sci.* **1973**, *29*, 1388−1393.
(12) Moras, D.; Metz, B.; Weiss, R. Structural Study on Cryptates 2. Crystal and Molecular Structure of Rubidium and Cesium Cryptates, C18H36N2.O6-RbSCN-H2O and C18H36N2O6-CsSCN-H2O. *Acta Crystallogr., Sect. B: Struct. Sci.* **1973**, *29*, 388−395.
(13) Chen, Q. Z.; Cannell, K.; Nicoll, J.; Dearden, D. V. The macrobicyclic cryptate effect in the gas phase. *J. Am. Chem. Soc.* **1996**, *118*, 6335−6344.
(14) Ralph, S. F.; Iannitti, P.; Kanitz, R.; Sheil, M. M. Determination of the relative stabilities of metal-antibiotic and metal-cryptand complexes by electrospray ionisation mass spectrometry. *Eur. Mass Spectrom.* **1996**, *2*, 173−179.
(15) Inokuchi, Y.; Boyarkin, O. V.; Kusaka, R.; Haino, T.; Ebata, T.; Rizzo, T. R. UV and IR Spectroscopic Studies of Cold Alkali Metal Ion-Crown Ether Complexes in the Gas Phase. *J. Am. Chem. Soc.* **2011**, *133*, 12256−12263.
(16) Inokuchi, Y.; Boyarkin, O. V.; Kusaka, R.; Haino, T.; Ebata, T.; Rizzo, T. R. Ion Selectivity of Crown Ethers Investigated by UV and IR Spectroscopy in a Cold Ion Trap. *J. Phys. Chem. A* **2012**, *116*, 4057−4068.
(17) Inokuchi, Y.; Ebata, T.; Rizzo, T. R. UV and IR Spectroscopy of Cold H2O+-Benzo-Crown Ether Complexes. *J. Phys. Chem. A* **2015**, *119*, 11113−11118.
(18) Inokuchi, Y.; Ebata, T.; Rizzo, T. R. Solvent Effects on the Encapsulation of Divalent Ions by Benzo-18-Crown-6 and Benzo-15-Crown-5. *J. Phys. Chem. A* **2015**, *119*, 8097−8105.
(19) Inokuchi, Y.; Ebata, T.; Rizzo, T. R. Microhydration of Dibenzo-18-Crown-6 Complexes with K+, RID+, and Cs+ Investigated by Cold UV and IR Spectroscopy in the Gas Phase. *J. Phys. Chem. A* **2018**, *122*, 3754−3763.
(20) Inokuchi, Y.; Ebata, T.; Rizzo, T. R. UV and IR Spectroscopy of Transition Metal-Crown Ether Complexes in the Gas Phase: Mn2+(benzo-15-crown-5)(H2O)(0-2). *J. Phys. Chem. A* **2019**, *123*, 6781−6786.
(21) Inokuchi, Y.; Ebata, T.; Rizzo, T. R.; Boyarkin, O. V. Microhydration Effects on the Encapsulation of Potassium Ion by Dibenzo-18-Crown-6. *J. Am. Chem. Soc.* **2014**, *136*, 1815−1824.
(22) Inokuchi, Y.; Kaneko, M.; Honda, T.; Nakashima, S.; Ebata, T.; Rizzo, T. R. UV and IR Spectroscopy of Cryogenically Cooled, Lanthanide-Containing Ions in the Gas Phase. *Inorg. Chem.* **2017**, *56*, 277−281.
(23) Inokuchi, Y.; Kusaka, R.; Ebata, T.; Boyarkin, O. V.; Rizzo, T. R. Laser Spectroscopic Study of Cold HostGuest Complexes of Crown Ethers in the Gas Phase. *ChemPhysChem* **2013**, *14*, 649−660.
(24) Kida, M.; Kubo, M.; Ujihira, T.; Ebata, T.; Abe, M.; Inokuchi, Y. Selective Probing of Potassium Ion in Solution by Intramolecular Excimer Fluorescence of Dibenzo-Crown Ethers. *ChemPhysChem* **2018**, *19*, 1331−1335.
(25) Kida, M.; Wada, K.; Muramatsu, S.; Shang, R.; Yamamoto, Y.; Inokuchi, Y. Spherand complexes with Li+ and Na+ ions in the gas phase: encapsulation structure and characteristic unimolecular dissociation. *Phys. Chem. Chem. Phys.* **2021**, *23*, 25029−25037.
(26) Dantz, D. A.; Buschmann, H. J.; Schollmeyer, E. Effects of the benzosubstitution of cryptands for the complex formation between protons, alkali and alkaline earth cations in water. *Polyhedron* **1998**, *17*, 1891−1895.
(27) Maqsood, N.; Asif, A.; Ayub, K.; Iqbal, J.; Elnaggar, A. Y.; Mersal, G. A. M.; Ibrahim, M. M.; El-Bahy, S. M. DFT study of alkali and alkaline earth metal-doped benzocryptand with remarkable NLO properties. *RSC Adv.* **2022**, *12*, 16029−16045.
(28) DeBlase, A. F.; Dziekonski, E. T.; Hopkins, J. R.; Burke, N. L.; Sheng, H. M.; Kenttamaa, H. I.; McLuckey, S. A.; Zwier, T. S. Alkali Cation Chelation in Cold beta-O-4 Tetralignol Complexes. *J. Phys. Chem. A* **2016**, *120*, 7152−7166.
(29) Burke, N. L.; DeBlase, A. F.; Redwine, J. G.; Hopkins, J. R.; McLuckey, S. A.; Zwier, T. S. Gas-Phase Folding of a Prototypical Protonated Pentapeptide: Spectroscopic Evidence for Formation of a Charge-Stabilized beta-Hairpin. *J. Am. Chem. Soc.* **2016**, *138*, 2849−2857.
(30) DeBlase, A. F.; Harrilal, C. P.; Lawler, J. T.; Burke, N. L.; McLuckey, S. A.; Zwier, T. S. Conformation-Specific Infrared and Ultraviolet Spectroscopy of Cold [YAPAA+H]+ and [YGPAA+H]+ Ions: A Stereochemical "Twist" on the β-Hairpin Turn. *J. Am. Chem. Soc.* **2017**, *139*, 5481−5493.
(31) Lawler, J. T.; Harrilal, C. P.; DeBlase, A. F.; Sibert, E. L.; McLuckey, S. A.; Zwier, T. S. Single-conformation spectroscopy of cold, protonated (D)PG-containing peptides: switching beta-turn types and formation of a sequential type II/II' double beta-turn. *Phys. Chem. Chem. Phys.* **2022**, *24*, 2095−2109.
(32) Rizzo, T. R.; Boyarkin, O. V. Cryogenic Methods for the Spectroscopy of Large, Biomolecular Ions. In *Gas-Phase Ir Spectroscopy and Structure of Biological Molecules*, Rijs, A. M.; Oomens, J., Eds.; Springer International Publishing: Switzerland, 2015; Vol. *364*, pp 43−97.
(33) Shannon, R. D. Revised Effective Ionic-Radii and Systematic Studies of Interatomic Distances in Halides and Chalcogenides. *Acta Crystallogr., Sect. A: Cryst. Phys., Diffr., Theor. Gen. Crystallogr.* **1976**, *32*, 751−767.
(34) Lehn, J. M.; Sauvage, J. P. 2-Cryptates-Stability and Selectivity of Alkali and Alkaline-Earth Macrobicyclic Complexes. *J. Am. Chem. Soc.* **1975**, *97*, 6700−6707.
(35) Inokuchi, Y.; Boyarkin, O. V.; Ebata, T.; Rizzo, T. R. UV and IR spectroscopy of cold 1,2-dimethoxybenzene complexes with alkali metal ions. *Phys. Chem. Chem. Phys.* **2012**, *14*, 4457−4462.
(36) Yi, J. T.; Ribblett, J. W.; Pratt, D. W. Rotationally Resolved Electronic Spectra of 1,2-Dimethoxybenzene and the 1,2-Dimethoxybenzene−Water Complex. *J. Phys. Chem. A* **2005**, *109*, 9456−9464.
(37) Sibert, E. L. Modeling vibrational anharmonicity in infrared spectra of high frequency vibrations of polyatomic molecules. *J. Chem. Phys.* **2019**, *150*, No. 090901.
(38) Buchanan, E. G.; Dean, J. C.; Zwier, T. S.; Sibert, E. L. Towards a first-principles model of Fermi resonance in the alkyl CH stretch region: Application to 1,2-diphenylethane and 2,2,2-paracyclophane. *J. Chem. Phys.* **2013**, *138*, No. 064308.
(39) Hewett, D. M.; Bocklitz, S.; Tabor, D. P.; Sibert, E. L.; Suhm, M. A.; Zwier, T. S. Identifying the first folded alkylbenzene via ultraviolet, infrared, and Raman spectroscopy of pentylbenzene through decylbenzene. *Chem. Sci.* **2017**, *8*, 5305−5318.
(40) Hewett, D. M.; Tabor, D. P.; Fischer, J. L.; Sibert, E. L.; Zwier, T. S. Infrared-Enhanced Fluorescence-Gain Spectroscopy: Conforma-

https://doi.org/10.1021/acs.jpca.3c03457
J. Phys. Chem. A 2023, 127, 6227−6240

tion-Specific Excited-State Infrared Spectra of Alkylbenzenes. *J. Phys. Chem. Lett.* **2017**, *8*, 5296−5300.
(41) Tabor, D. P.; Hewett, D. M.; Bocklitz, S.; Korn, J. A.; Tomaine, A. J.; Ghosh, A. K.; Zwier, T. S.; Sibert, E. L. Anharmonic modeling of the conformation-specific IR spectra of ethyl, n-propyl, and n-butylbenzene. *J. Chem. Phys.* **2016**, *144*, No. 224310.
(42) Sibert, E. L.; Kidwell, N. M.; Zwier, T. S. A First-Principles Model of Fermi Resonance in the Alkyl CH Stretch Region: Application to Hydronaphthalenes, Indanes, and Cyclohexane. *J. Phys. Chem. B* **2014**, *118*, 8236−8245.
(43) Sibert, E. L.; Tabor, D. P.; Kidwell, N. M.; Dean, J. C.; Zwier, T. S. Fermi Resonance Effects in the Vibrational Spectroscopy of Methyl and Methoxy Groups. *J. Phys. Chem. A* **2014**, *118*, 11272−11281.
(44) Kidwell, N. M.; Mehta-Hurt, D. N.; Korn, J. A.; Sibert, E. L.; Zwier, T. S. Ground and excited state infrared spectroscopy of jet-cooled radicals: Exploring the photophysics of trihydronaphthyl and inden-2-ylmethyl. *J. Chem. Phys.* **2014**, *140*, No. 214302.
(45) Korn, J. A.; Tabor, D. P.; Sibert, E. L.; Zwier, T. S. Conformation-specific spectroscopy of alkyl benzyl radicals: Effects of a radical center on the CH stretch infrared spectrum of an alkyl chain. *J. Chem. Phys.* **2016**, *145*, No. 124314.
(46) Buchanan, E. G.; Sibert, E. L.; Zwier, T. S. Ground State Conformational Preferences and CH Stretch-Bend Coupling in a Model Alkoxy Chain: 1,2-Diphenoxyethane. *J. Phys. Chem. A* **2013**, *117*, 2800−2811.
(47) Zhang, C.; Chen, H. W.; Guymon, A. J.; Wu, G. X.; Cooks, R. G.; Ouyang, Z. Instrumentation and methods for ion and reaction monitoring using a non-scanning rectilinear ion trap. *Int. J. Mass Spectrom.* **2006**, *255*−*256*, 1−10.
(48) Paizs, B.; Suhai, S. Comparative study of BSSE correction methods at DFT and MP2 levels of theory. *J. Comput. Chem.* **1998**, *19*, 575−584.
(49) Walker, B.; Liu, C. W.; Wait, E.; Ren, P. Y. Automation of AMOEBA polarizable force field for small molecules: Poltype 2. *J. Comput. Chem.* **2022**, *43*, 1530−1542.
(50) Marcus, Y. Thermodynamics of solvation of ions. 5. Gibbs free-energy of hydration at 298.15-K. *J. Chem. Soc., Faraday Trans.* **1991**, *87*, 2995−2999.
(51) Jing, Z. F.; Rackers, J. A.; Pratt, L. R.; Liu, C. W.; Rempe, S. B.; Ren, P. Y. Thermodynamics of ion binding and occupancy in potassium channels. *Chem. Sci.* **2021**, *12*, 8920.
(52) Kim, S.; Chen, J.; Cheng, T.; Gindulyte, A.; He, J.; He, S.; Li, Q.; Shoemaker, B. A.; Thiessen, P. A.; Yu, B.; et al. PubChem 2023 update. *Nucleic Acids Res.* **2023**, *51*, D1373−D1380.
(53) Romo, T. D.; Leioatts, N.; Grossfield, A. Lightweight Object Oriented Structure Analysis: Tools for Building Tools to Analyze Molecular Dynamics Simulations. *J. Comput. Chem.* **2014**, *35*, 2305−2318.
(54) Frisch, M. J.; Trucks, G. W.; Schlegel, H. B.; Scuseria, G. E.; Robb, M. A.; Cheeseman, J. R.; Scalmani, G.; Barone, V.; Petersson, G. A.; Nakatsuji, H.; et al. *Gaussian 16*, revision C.01; Gaussian Inc.: Wallingford, CT, 2016.
(55) Chaudhari, M. I.; Vanegas, J. M.; Pratt, L. R.; Muralidharan, A.; Rempe, S. B. Hydration Mimicry by Membrane Ion Channels. *Ann. Rev. Phys. Chem.* **2020**, *71*, 461−484.
(56) Rempe, S. B.; Asthagiri, D.; Pratt, L. R. Inner shell definition and absolute hydration free energy of K+(aq) on the basis of quasi-chemical theory and ab initio molecular dynamics. *Phys. Chem. Chem. Phys.* **2004**, *6*, 1966−1969.
(57) Chaudhari, M. I.; Soniat, M. L.; Rempe, S. B. Octa-Coordination and the Aqueous Ba2+ Ion. *J. Phys. Chem. B* **2015**, *119*, 8746−8753.
(58) Cheng, X. L.; Steele, R. P. Efficient anharmonic vibrational spectroscopy for large molecules using local-mode coordinates. *J. Chem. Phys.* **2014**, *141*, No. 104105.
(59) Cheng, X. L.; Talbot, J. J.; Steele, R. P. Tuning vibrational mode localization with frequency windowing. *J. Chem. Phys.* **2016**, *145*, No. 124112.
(60) Jacob, C. R.; Reiher, M. Localizing normal modes in large molecules. *J. Chem. Phys.* **2009**, *130*, No. 084106.
(61) Sibert, E. L. Dressed local mode Hamiltonians for CH stretch vibrations. *Mol. Phys.* **2013**, *111*, 2093−2099.
(62) Weymuth, T.; Jacob, C. R.; Reiher, M. A Local-Mode Model for Understanding the Dependence of the Extended Amide III Vibrations on Protein Secondary Structure. *J. Phys. Chem. B* **2010**, *114*, 10649−10660.
(63) Zimmerman, P. M.; Smereka, P. Optimizing Vibrational Coordinates To Modulate Intermode Coupling. *J. Chem. Theory Comput.* **2016**, *12*, 1883−1891.
(64) Patwari, G. N.; Lisy, J. M. Cyclohexane as a Li+ Selective Ionophore. *J. Phys. Chem. A* **2007**, *111*, 7585−7588.
(65) Sibert, E. L.; Tabor, D. P.; Lisy, J. M. Modeling the CH Stretch Vibrational Spectroscopy of M+ Cyclohexane (M = Li, Na, and K) Ions. *J. Phys. Chem. A* **2015**, *119*, 10293−10299.
(66) Armentrout, P. B.; Austin, C. A.; Rodgers, M. T. Alkali metal cation interactions with 12-crown-4 in the gas phase: Revisited. *Int. J. Mass Spectrom.* **2012**, *330*−*332*, 16−26.
(67) Tuttle, W. D.; Gardner, A. M.; Andrejeva, A.; Kemp, D. J.; Wakefield, J. C. A.; Wright, T. G. Consistent assignment of the vibrations of symmetric and asymmetric ortho-disubstituted benzenes. *J. Mol. Spectrosc.* **2018**, *344*, 46−60.
(68) Henrichs, C.; Hebestreit, M. L.; Krugler, D.; Schmitt, M. Structural changes upon electronic excitation in 1,2-dimethoxybenzene from Franck-Condon fits of the fluorescence emission spectra. *J. Mol. Struct.* **2020**, *1211*, No. 127855.
(69) Wolfe, S.; Schlegel, H. B.; Whangbo, M. H.; Bernardi, F. Origin of Bohlmann Bands. *Can. J. Chem.* **1974**, *52*, 3787−3792.
(70) Glendening, E. D.; Weinhold, F. Natural Resonance Theory: II. Natural bond order and valency. *J. Comput. Chem.* **1998**, *19*, 610−627.

https://doi.org/10.1021/acs.jpca.3c03457
J. Phys. Chem. A 2023, 127, 6227−6240